



HAL
open science

Reactive Solubilization of Heterometallic Clusters by Treatment of (TrBi 3) 2– Anions (Tr=Ga, In, Tl) with [MnN(SiMe 3) 2 2]

Julia Rienmüller, Andreas Schmidt, Nathan J Yutronkie, Rodolphe Clérac, C Gunnar Werncke, Florian Weigend, Stefanie Dehnen

► **To cite this version:**

Julia Rienmüller, Andreas Schmidt, Nathan J Yutronkie, Rodolphe Clérac, C Gunnar Werncke, et al.. Reactive Solubilization of Heterometallic Clusters by Treatment of (TrBi 3) 2– Anions (Tr=Ga, In, Tl) with [MnN(SiMe 3) 2 2]. *Angewandte Chemie International Edition*, 2022, 61 (42), 10.1002/anie.202210683 . hal-03821174

HAL Id: hal-03821174

<https://hal.science/hal-03821174>

Submitted on 19 Oct 2022

HAL is a multi-disciplinary open access archive for the deposit and dissemination of scientific research documents, whether they are published or not. The documents may come from teaching and research institutions in France or abroad, or from public or private research centers.

L'archive ouverte pluridisciplinaire **HAL**, est destinée au dépôt et à la diffusion de documents scientifiques de niveau recherche, publiés ou non, émanant des établissements d'enseignement et de recherche français ou étrangers, des laboratoires publics ou privés.

Zintl Anions

Reactive Solubilization of Heterometallic Clusters by Treatment of $(\text{TrBi}_3)^{2-}$ Anions (Tr = Ga, In, Tl) with $[\text{Mn}\{\text{N}(\text{SiMe}_3)_2\}_2]$

Julia Rienmüller, Andreas Schmidt, Nathan J. Yutronkie, Rodolphe Clérac, C. Gunnar Werncke,* Florian Weigend,* and Stefanie Dehnen*

How to cite: *Angew. Chem. Int. Ed.* **2022**, *61*, e202210683

International Edition: doi.org/10.1002/anie.202210683

German Edition: doi.org/10.1002/ange.202210683

Abstract: Lowering the charge of Zintl anions by (element-)organic substituents allows their use as sources of (semi)metal nanostructures in common organic solvents, as realized for group 15 anions or Ge_9^{4-} and Sn_9^{4-} . We developed a new strategy for other anions, using low-coordinate 3d metal complexes as electrophiles. $[\text{K}(\text{crypt-222})]^+$ salts of $(\text{TrBi}_3)^{2-}$ anions dissolved in situ in Et_2O and/or THF when reacted with $[\text{Mn}(\text{hmds})_2]$. Work-up afforded soluble $[\text{K}(\text{crypt-222})]^+$ salts of $[\{(\text{hmds})_2\text{Mn}\}_2(\text{TlBi}_3)]^{2-}$ (in **1**), $[\{(\text{hmds})_2\text{Mn}\}_2(\text{Bi}_2)]^{2-}$ (in **2**), and $[\{(\text{hmds})\text{Mn}\}_4(\text{Bi}_2)_2]^{2-}$ (in **3**) (crypt-222 = 4,7,13,16,21,24-hexaoxa-1,10-diazabicyclo-[8.8.8]hexacosane; Tr = Ga, In, Tl; hmds = $\text{N}(\text{SiMe}_3)_2$), representing rare cases of Zintl clusters with open-shell metal atoms. **1** comprises the first coordination compound of the $(\text{TlBi}_3)^{2-}$ anion, **2** features a diamond-shaped $\{\text{Pn}_2\text{M}_2\}$ unit, and **3** is a mixed-valent $\text{Mn}^{\text{I}}/\text{Mn}^{\text{II}}$ compound. The uncommon electronic structures in **1–3** and magnetic coupling were studied by comprehensive DFT calculations.

Introduction

In recent years, Zintl anions have been proven excellent starting materials of heterometallic and intermetallic clusters, in which p-block (semi)metal atoms are combined with d-block or f-block metal atoms.^[1–5] However, owing to

their intrinsic anionic charges and sensitivities, the access and further treatment of such species have been widely restricted to very few, highly basic solvents—ethane-1,2-diamine (en), liquid ammonia, or N,N-dimethylformamide (dmf). The attachment of elementorganic or organic groups served to lower the negative charge, and therefore allowed for solubility in common solvent like THF or CH_3CN . This has been extensively applied to Zintl anions of group 15 elements,^[6] and later on, in 2007, also for Zintl anions of group 14 elements with their intrinsically higher charge per atom.^[3,7] Some years later, in 2012, full compensation of the charge even allowed for water solubility and compatibility, which opened up new options for subsequent reactions.^[8] However, so far, such modifications have only been feasible for the homoatomic Zintl anions Ge_9^{4-} and Sn_9^{4-} .

Another way of lowering the charge, which was successfully applied to Ge_9^{4-} and Sn_9^{4-} ,^[9–11] but also to Si_4^{4-} , Ge_4^{4-} , $(\text{Si}_x\text{Ge}_x)^{4-}$, and Sn_4^{4-} , with even higher charges per atom, is the use of Zintl anions as ligands of transition metal complexes; in these cases, the nine-atom or four-atom cages act as Lewis bases that replace one or more of the original ligands of the transition metal complex. Products of such reactions have been combinations of said Zintl anions with group 6 metal carbonyl complex fragments $\{\text{M}(\text{CO})_3\}$ (M = Cr, Mo, W)^[12] and d^7 or d^{10} metal complex fragments, such as $\{\text{Ir}(\text{cod})\}$, $\{\text{CuL}\}$ (L = Mes, NHC^{Dipp} , P^{Pr_3} , PCy_3), $\{\text{PdPPh}_3\}$, $\{\text{ZnL}\}$ (L = Ph, Mes, ^iPr) or $\{\text{CdL}\}$ (L = Ph, Sn^nBu_3) units,^[9–11,13–15] or with “naked” cations of groups 11 and 12.^[13,15–17] Some of the latter have also been applied to binary Zintl anions, which have been reported to form anions like $[(\text{PhZn})_2(\text{Sn}_2\text{Sb}_5)]^{3-}$,^[18] $[\{(\text{cod})\text{Ru}\}(\text{Tl}_2\text{Bi}_6)]^{2-}$ (cod = 1,5-cyclooctadiene)^[19] with remaining organic ligands, as well as $[\text{Au}(\text{Sn}_2\text{Sb}_2)]^{3-}$ and the one-dimensional strand $[\{\text{Au}(\text{TlSn}_3)\}^{4-}]_n$ without ligands.^[17,20] All of these species actually represent bridges to the heterometallic and intermetallic clusters mentioned above because they do not differ from the original Zintl anions regarding their solubility, and thus will not be detailed here.^[1–5]

In summary, binary anions with group 13/15 or group 14/15 elemental combinations could not yet be systematically transferred into well-soluble derivatives with organic shielding. For $[\text{K}(\text{crypt-222})]^+$ salts of $(\text{TrBi}_3)^{2-}$ anions (crypt-222 = 4,7,13,16,21,24-hexaoxa-1,10-diazabicyclo-[8.8.8]hexacosane; Tr = Ga, In, Tl), one of the underlying problems is the inclination of $(\text{TrBi}_3)^{2-}$ to undergo redox processes, in which the formally negatively charged Tr atoms are released as elemental metals, while polybismuthide units would be integrated in usually ligand-free cluster

[*] J. Rienmüller, A. Schmidt, Dr. C. G. Werncke, Prof. F. Weigend, Prof. Dr. S. Dehnen
 Fachbereich Chemie und Wissenschaftliches Zentrum für Materialwissenschaften (WZMW),
 Philipps-Universität Marburg
 Hans-Meerwein-Str. 4, 53043 Marburg (Germany)
 E-mail: gunnar.werncke@chemie.uni-marburg.de
 florian.weigend@chemie.uni-marburg.de
 dehnen@chemie.uni-marburg.de

Dr. N. J. Yutronkie, Dr. R. Clérac
 Univ. Bordeaux, CNRS, Centre de Recherche Paul Pascal, CRPP,
 UMR 5031
 33600 Pessac (France)

© 2022 The Authors. Angewandte Chemie International Edition published by Wiley-VCH GmbH. This is an open access article under the terms of the Creative Commons Attribution License, which permits use, distribution and reproduction in any medium, provided the original work is properly cited.

molecules;^[21] thus the choice of a suitable reactant must be done with even greater care.

In the light of the described state-of-the-art, we recognize an obvious lack of highly versatile synthetic approaches in common solvents. However, such methods would provide significant benefit for multimetallic cluster syntheses in general. Inspired by this and by the corresponding experimental challenge, we developed a new way of shielding Zintl anions, which we report herein. Our synthetic strategy is based on the idea of using the two-coordinate transition metal complex $[\text{Mn}(\text{hmds})_2]$ ($\text{hmds} = \text{N}(\text{SiMe}_3)_2$) as strong, yet electrochemically relatively inert, electrophiles for attachment to Zintl anions.

Results and Discussion

A suspension of $[\text{K}(\text{crypt-222})]_2(\text{TrBi}_3)\cdot\text{en}$ ($\text{Tr} = \text{Ga}, \text{In}, \text{Tl}$) in THF or $\text{Et}_2\text{O}/\text{THF}$ mixtures (v:v=1:1) immediately turned dark brown upon addition of $[\text{Mn}(\text{hmds})_2]$, indicating reactive dissolution of the Zintl salt (see Figure 1).

From such solutions, we obtained the novel compounds $[\text{K}(\text{crypt-222})]_2\{[(\text{hmds})_2\text{Mn}]_2(\text{TlBi}_3)\} \cdot 1.5 \text{Et}_2\text{O}$ (**1**·1.5 Et_2O),

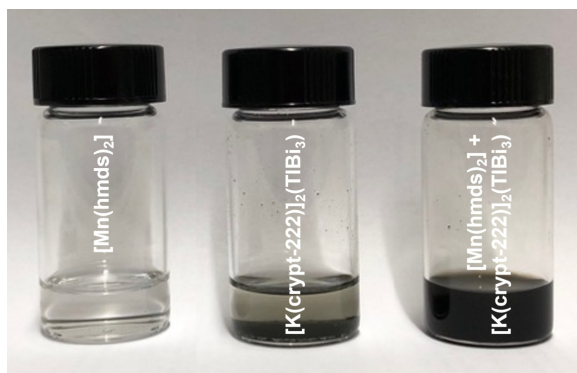
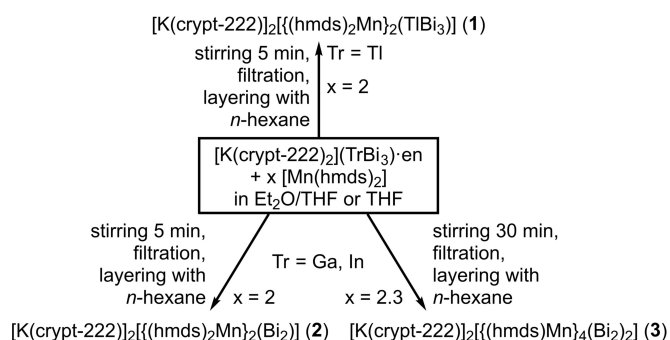


Figure 1. Photographs illustrating the behavior of the reactants in THF: solution of $[\text{Mn}(\text{hmds})_2]$ in THF (left), suspension of $[\text{K}(\text{crypt-222})]_2(\text{TlBi}_3)\cdot\text{en}$ in THF (center) and reactive solution of $[\text{Mn}(\text{hmds})_2] + [\text{K}(\text{crypt-222})]_2(\text{TlBi}_3)\cdot\text{en}$ in THF (right).



Scheme 1. Non-stoichiometric reaction schemes for the syntheses of **1**–**3**. Crystal solvent is not indicated here for clarity. The nature and amount of crystal solvents are given in the text. For more details see the Supporting Information.

$[\text{K}(\text{crypt-222})]_2\{[(\text{hmds})_2\text{Mn}]_2(\text{Bi}_2)\} \cdot 4 \text{THF}$ (**2**·4 THF), and $[\text{K}(\text{crypt-222})]_2\{[(\text{hmds})\text{Mn}]_4(\text{Bi}_2)_2\}$ (**3**) upon filtration and layering with *n*-hexane, as summarized in Scheme 1.

All three compounds were investigated by means of single-crystal X-ray diffraction^[22] and by elemental analyses using micro-X-ray fluorescence spectroscopy ($\mu\text{-XFS}$), which confirmed their composition (see Supporting Information). In contrast, electrospray-ionization mass spectrometry (ESI-MS) was not successful on any of these compounds—including the complex $[\text{Mn}(\text{hmds})_2]$ itself that was used for the reactions—in spite of many attempts and a lot of experience we have with this method. In the mass spectra, we see fragments only; this clearly indicates the high tendency of hmds-decorated molecules towards decomposition under ESI-MS conditions.

The molecular structures of the anion in compounds **1** and **2** are shown in Figure 2. Supplementary crystallographic figures are provided in the Supporting Information. The anion in **1** consists of a disordered $(\text{TlBi}_3)^{2-}$ tetrahedron which coordinates in a $\text{trans-}\eta^2\text{-}\eta^2$ fashion to two $[\text{Mn}(\text{hmds})_2]$ units. The atomic distances within the *pseudo*-tetrahedron are between 2.907(4) and 3.314(5) Å, with the longest distances observed at the edges that bind to the formally neutral $[\text{Mn}(\text{hmds})_2]$ units. The distances are elongated on average in comparison with the free $(\text{TlBi}_3)^{2-}$ anion (3.04589(7)–3.0772(6) Å),^[19] which again reflects the involvement of the electrons from bonding orbitals in the coordination of the metal complexes. The $[\text{Mn}(\text{hmds})_2]$ unit as a whole was attached to the $(\text{TlBi}_3)^{2-}$ anion without affecting its charge. The much better solubility of the resulting molecule is thus solely due to the four terminal SiMe_3 groups.

While the $(\text{TlBi}_3)^{2-}$ anion remained intact during formation of **1**, the $(\text{GaBi}_3)^{2-}$ and $(\text{InBi}_3)^{2-}$ anions fragmented upon electrophilic attack, despite an entirely analogous reaction. Instead, both decomposed to yield elemental Ga or In, and a Bi_2^{2-} dumbbell. Under the workup conditions indicated in Scheme 1, this Bi_2^{2-} unit $\mu\text{-}\eta^2$ -bridges two $[\text{Mn}(\text{hmds})_2]$ units, again forming a well-soluble molecular complex in **2**. The uncoordinated Bi_2^{2-} anion observed in $[\text{K}(\text{crypt-222})]_2\text{Bi}_2$ formally possesses a double bond, with a Bi–Bi distance of 2.8377(7) Å,^[23] which is expanded in **2** to 2.90222(18) Å. This observation can be explained by the twofold side-on-coordination of the Mn^{2+} ions and a corresponding decrease of the bond order.

The described different behavior of these binary Zintl anions is in line with the observations reported in previous studies, in which the tendency to include the group 13 element in the products cluster decreases with decreasing atomic number ($\text{Tl} > \text{In} > \text{Ga}$). A molecular structure of the $(\text{GaBi}_3)^{2-}$ anion indeed has never been crystallographically determined (while the anion was detected by mass spectrometry),^[24] but it is supposed to be isostructural to the known $(\text{InBi}_3)^{2-}$ and $(\text{TlBi}_3)^{2-}$ anions.^[25,19] Besides this anion, two larger anions have recently been reported, $(\text{Ga}_2\text{Bi}_{16})^{4-}$ and $[\text{Bi}@\text{Ga}_8(\text{Bi}_2)_6]^{3-/5-}$,^[24] with the latter being similar to $[\text{Bi}@\text{In}_8(\text{Bi}_2)_6]^{3-/5-}$.^[26] Calculations revealed that $(\text{GaBi}_3)^{2-}$ is at the extreme limit of isolatable *pseudo*-tetrahedral anions due to geometrical aspects, while this is

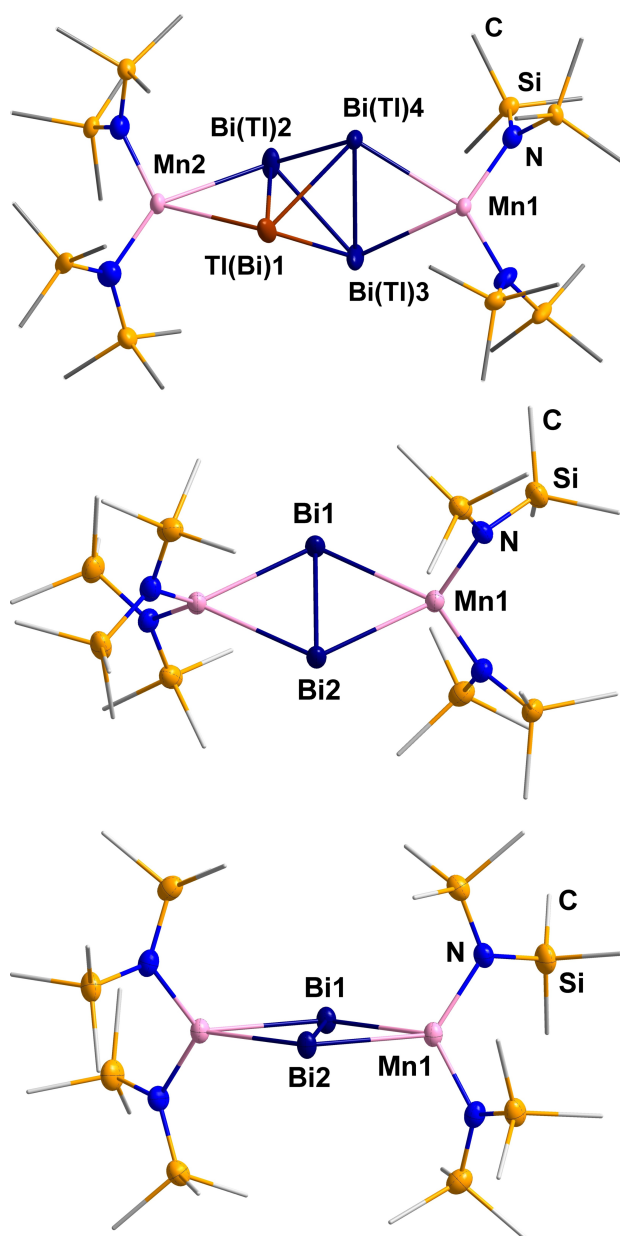


Figure 2. Molecular structures of the anions in compounds **1** (top) and **2** (two views: center and bottom), with Bi, Mn, N, and Si atoms shown as thermal ellipsoids with 50% probability, C atoms are drawn as wires, H atoms are omitted for clarity. The anion in **1** shows a statistical disorder of the $\{\text{TlBi}_3\}$ unit that was modeled with two sets of split positions. As Tl and Bi atoms cannot be distinguished by standard X-ray diffraction experiments, all involved sites were assigned a 0.125 occupancy by Tl atoms and a 0.375 occupancy by Bi atoms. For clarity, we illustrate only one of these sets here, with one of the atoms being randomly picked to represent the Tl atom (see Supporting Information for more details). Selected distances in **1** [Å]: Bi–(Tl)Bi 2.907(4)–3.311(3), Bi(Tl)–Mn 2.967(3)–3.097(3), Mn–N 2.037(3)–2.051(3). Selected distances in **2** [Å]: Bi–Bi 2.90222(18), Bi–Mn 2.9616(3)–2.9712(3), Mn–N 2.0659(19)–2.0692(18).

less problematic for $(\text{InBi}_3)^{2-}$ and not a problem at all for $(\text{TlBi}_3)^{2-}$ due to more similar atomic sizes.^[27] Consequently, only few clusters have so far been reported, in which Ga or In and Bi coexist, such as $[\text{Sm}@\text{Ga}_{3-x}\text{H}_{3-2x}\text{Bi}_{10+x}]^{3-}$ ($x=0$,

1)^[28] or $\{[\text{La}@\text{In}_2\text{Bi}_{11}]_2\text{Bi}_2\}^{6-}$,^[29] while there are several examples for the TlBi-elemental combination. These were reported as salts of binary anions, like $[\text{K}(\text{crypt-222})]_2(\text{TlBi}_3)$, $[\text{K}(\text{crypt-222})]_3(\text{Tl}_4\text{Bi}_5)$, and $[\text{K}(\text{crypt-222})]_3(\text{Tl}_4\text{Bi}_3)$,^[30] or as salts of ternary clusters like $\{[\text{Ru}(\text{cod})]_4\text{Bi}_{18}\}^{4-}$, $[\text{U}@\text{Bi}_{12}]^{3-}$, $[\text{Th}@\text{Bi}_{12}]^{4-}$, $\{[\text{Ru}(\text{cod})]\text{Tl}_2\text{Bi}_6\}^{2-}$, $[\text{U}@\text{Tl}_2\text{Bi}_{11}]^{3-}$, or $[\text{Th}@\text{Tl}_2\text{Bi}_{11}]^{3-}$, which were obtained from reactions of $(\text{TlBi}_3)^{2-}$ with d-block or f-block metal compounds $[\text{Ru}(\text{cod})\{\text{H}_2\text{CC}(\text{Me})\text{CH}_2\}_2]$, $[\text{UCp}^\#_3]$ or $[\text{ThCp}^\#_3]\text{Cl}$, for instance.^[19,31,24]

We were interested to get insight into the bonding situations of the anions in compounds **1** and **2**. For this, density functional theory (DFT) calculations^[32] were carried out with the TPSSh functional^[33] and def2-TZVP basis sets.^[34] In all calculations the conductor-like screening model was employed for charge compensation.^[35] For exploring the binding energy (E_B) between $(\text{TlBi}_3)^{2-}$ and two $[\text{Mn}(\text{hmds})_2]$ units in the anion of **1**, we calculated the difference of the total energy of **1** and the total energies of said units. E_B amounts to $-69.2 \text{ kJ mol}^{-1}$ (thus $-34.6 \text{ kJ mol}^{-1}$ per side), both for a high-spin state (hs; $S=5$) and for the broken-symmetry low-spin state (bs; $S=0$). This indicates a negligible coupling between the $S=5/2$ Mn^{II} spins. In addition, we find that the interaction between $(\text{TlBi}_3)^{2-}$ and Mn is highly ionic in nature. This is evident when replacing $(\text{TlBi}_3)^{2-}$ with isoelectronic but neutral Bi_4 which results in an even slightly positive binding energy ($+3.5 \text{ kJ mol}^{-1}$). The Tl–Bi bonds within the *pseudo*-tetrahedral subunit are strongly polarized. About 75% of the Mulliken charge in the corresponding localized orbitals is assigned to Bi, and 25% to Tl—in agreement with the higher electronegativity of Bi (1.67) as compared to Tl (1.44).^[36] The electronic overload at the Bi atoms is partly transferred to the attached $[\text{Mn}(\text{hmds})_2]$ units, as indicated by the change in the average Mulliken charge of Bi from -0.57 in $(\text{TlBi}_3)^{2-}$ to -0.38 in **1**, as well as in the average Mulliken number of unpaired electrons for Mn being reduced from 5.02 for an isolated $[\text{Mn}(\text{hmds})_2]$ complex to 4.89 in **1**.

The binding energy between Bi_2^{2-} and the two $[\text{Mn}(\text{hmds})_2]$ units in the anion of **2** amounts to $-156.1 \text{ kJ mol}^{-1}$ (-78 kJ mol^{-1} per side) for the high-spin state (a second conformer with a broken-symmetry low-spin state is disfavored by 6.7 kJ mol^{-1} , see also below). As discussed for **1**, the Bi_2^{2-} unit and the two $[\text{Mn}(\text{hmds})_2]$ moieties also undergo mainly ionic interactions, evident from the slightly positive E_B ($+14.6 \text{ kJ mol}^{-1}$) for isoelectronic but neutral Te_2 . The electronic overload is again transferred to the Mn atoms, evident from the reduction of the Mulliken charge at Bi from -1 in parent Bi_2^{2-} to -0.58 in **2**, and a reduction of the Mulliken number of unpaired electrons at the Mn atoms to 4.69. The charge transfer is also visible from the delocalization of the in-plane parts of the π and π^* orbitals of Bi_2^{2-} to the s and d orbitals of the two Mn atoms, as shown for the π^* orbitals in Figure 3. The concomitant reduction of the Bi–Bi bond order (Wiberg indices: 1.99 in Bi_2^{2-} , 1.31 in the anion of **2**) agrees well with a slightly increased Bi–Bi distance both in the calculation (by 0.034 \AA) and the experiment (by 0.065 \AA) relative to the

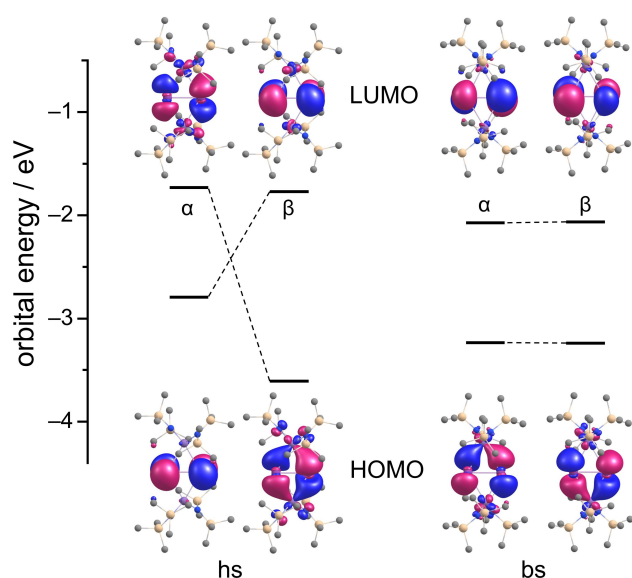


Figure 3. Frontier molecular spin orbitals of the anion in **2** for the high-spin (hs) and the broken-symmetry (bs) case. Amplitudes are drawn at ± 0.035 a.u.. For hs, α refers to the majority spin, that is, for the spin of the d electrons at the Mn atoms.

bond length in Bi_2^{2-} (calculated: 2.844 Å, experiment: 2.838 Å).^[23]

It is noteworthy that planar, diamond-shaped $\{\text{Pn}_2\text{M}_2\}$ units including heavier pnictogen ($\text{Pn}=\text{As}\cdots\text{Bi}$) and transition metal atoms are extremely rare,^[37] most likely owing to the reducing power of the Pn_2^{2-} dianions, which prefers to end up with a pyramidal coordination environment and formally zero charge of the Pn atoms. Accordingly, the planar $\{\text{Pn}_2\text{M}_2\}$ motif was rather observed for some rare-earth and actinide complexes with reductively resistant metal ions and thus mainly ionic interactions ($\{\text{Sm}^{\text{III}}_2\text{Pn}_2\}$ for $\text{Pn}=\text{Bi}$,^[38] Sb ,^[39] As ,^[40] and $\{\text{U}^{\text{IV}}_2\text{As}_2\}$).^[41] The more common motif for dinuclear transition metal compounds bearing a $\{\mu\text{-}\eta^2\text{-Pn}_2\}$ ligand is a butterfly-shaped $\{\text{Pn}_2\text{M}_2\}$ unit, which allows for additional M–M interactions (especially between low-valent M atoms like in carbonyl/cyclopentadienide complexes $[\{\text{Cp}^{\text{Me}}(\text{CO})_2\text{Mo}\}_2(\mu\text{-Bi}_2)]$ ^[42] and $[\{\text{Cp}(\text{CO})_2\text{Mo}\}_2(\mu\text{-Sb}_2)]$ ^[43] or for a formulation as a bridging Pn_2^{4-} unit, as in $[\{(\text{Ph}_3\text{P})_2\text{Pd}\}(\mu\text{-As}_2)]$ ^[44] and $[\{(\text{NHC})(\text{CO})\text{Ni}\}_2(\mu\text{-As}_2)]$.^[45] Given the scarcity of paramagnetic $\{\text{Pn}_2\text{M}_2\}$ complexes, magnetic studies on those with open-shell metal ions are unsurprisingly absent. For a related $\{\text{Zr}^{\text{III}}_2\text{N}_2\}$ motif bearing a bridging N_2^{2-} unit, strong antiferromagnetic coupling was proposed,^[46] whereas in some paramagnetic rare-earth $\{\text{M}_2\text{N}_2\}$ compounds ($\text{M}=\text{Gd}$, Dy , Tb), the antiferromagnetic coupling is considerably weaker.^[47]

We were therefore interested to explore how the planar $\{\text{Mn}_2\text{Bi}_2\}$ unit would behave in this regard—and whether a (hypothetical) bent isomer would show different properties. DFT calculations indicated that beside the planar conformer, also a slightly bent conformer (dihedral angle 169.1°) can be observed for different magnetic situations. While the planar system results from a ferromagnetic coupling of the two ions, with an $S=5$ high-spin (hs) ground

state, the bent conformer accords with antiferromagnetic coupling and a corresponding $S=0$ broken symmetry (bs) low-spin ground state. Both species are local minima on the energy hypersurface, with the experimentally observed planar conformer being very slightly preferred, by 4.2 kJ mol^{-1} . This indicates that the coupling is weak. Furthermore, the energy surface exhibits a moderate curvature for this degree of freedom: forcing the broken-symmetry state to planar shape requires 25.1 kJ mol^{-1} , and forcing the high-spin state to bent shape requires 9.3 kJ mol^{-1} only. Nevertheless, the two different coupling modes have impact on the shape of the frontier orbitals. In both cases, both HOMO and LUMO are dominated by the Bi_2^{2-} π^* orbitals, just like for the bare Bi_2^{2-} unit. For the slightly bent broken symmetry case (right hand side of Figure 3), the HOMOs of both spin types are the in-plane π^* orbitals. One observes delocalization towards the empty Mn(d) spin minority orbitals: for the α -spin π^* to the upper Mn atom with empty α -spin (and occupied β -spin) d orbitals, and for the β -spin π^* to the lower Mn atom with empty β -spin (and occupied α -spin) d orbitals. For the high-spin case in contrast, delocalization to empty Mn(d) orbitals is possible only for the minority spin, β . As a consequence, the in-plane α -spin π^* orbital is significantly higher in energy than its β -spin counterpart and also higher in energy than the α -spin π^* orbital perpendicular to the plane. Hence, for this state the HOMOs are the majority-spin π^* orbital perpendicular to the $\{\text{Bi}_2\text{Mn}_2\}$ plane and the minority-spin in-plane π^* orbital.

Despite many attempts on five different batches of **2** (see Supporting Information), the final experimental proof of the planar structure to exhibit a (weak) ferromagnetic coupling is still elusive, as the compounds are too sensitive as to produce reliable magnetic susceptibility (χ) data. We took great care while isolating, shipping, and preparing the samples for these measurements, but to date, none of the measurements delivered reproducible and physically meaningful results. The χT product at room temperature was found systematically lower than the expected value (8.75 $\text{cm}^3 \text{K mol}^{-1}$) for two isolated $S=5/2$ Mn^{II} spins (ranging from 6.4 and 7.9 $\text{cm}^3 \text{K mol}^{-1}$). Nevertheless, these experimental values, even if lower, strongly support the oxidation and spin states of the Mn metal ions. In all the samples, the χT product decreases when lowering the temperature. This indicates the presence of dominating antiferromagnetic interactions with a magnitude that varies strongly for the different batches—most probably owing to the dominance of impurities or decomposition products with much stronger (antiferromagnetic) coupling between the Mn magnetic centers. While we could selectively produce one of the decomposition products, $[\text{K}(\text{crypt-222})][\text{Mn}(\text{hmds})_3]$,^[48] and investigate its magnetic susceptibility, as well as for the reactant $[\text{Mn}(\text{hmds})_2]$ (both showing very weak antiferromagnetic couplings), these results did not allow us to draw additional conclusions on the magnetic properties of **2**. So at this stage, we suggest from the calculations that a weak ferromagnetic coupling might be present in the uncommon anion in **2**, but we need to refer to future work for a direct experimental proof of it.

The impact of available d orbitals on the structural features of the anion in **2** became evident by replacing the Mn atoms computationally with Zn that has no open d orbitals. This resulted in a switch from the side-on to an end-on bridging Bi_2^{2-} unit in a Zn–Bi–Bi–Zn zig-zag conformation (see Figure S8). A calculation of the Zn species starting with a structure according to the one observed in compound **2** does not converge into a local minimum without symmetry restrictions. With symmetry restrictions, a local minimum structure is obtained that is energetically disfavored by 48 kJ mol^{-1} with regard to the end-on isomer.

Stirring a suspension of $[\text{K}(\text{crypt-222})]_2(\text{GaBi}_3) \cdot \text{en}$ or $[\text{K}(\text{crypt-222})]_2(\text{InBi}_3) \cdot \text{en}$ in THF with $[\text{Mn}(\text{hmds})_2]$ for 30 minutes instead of 5 minutes (as for the formation of **2**) before layering of the filtrate with *n*-hexane yielded crystals of compound **3**. The molecular structure of the anion in **3** is illustrated in Figure 4 (Supplementary crystallographic figures are provided in the Supporting Information).

Two Bi_2^{2-} dumbbells act as $\eta^2\text{-}\eta^2\text{-}\eta^2\text{-}\mu^3$ -bridge to a zig-zag-shaped $[\text{Mn}(\text{hmds})_4]^{2+}$ unit. Alternatively, the structure of the 8-atom cluster can be described as two $\{\text{Bi}_2\text{Mn}_3\}$ pseudo-trigonal bipyramids that are fused by sharing one Mn–Mn edge and being surrounded by four $(\text{hmds})^-$ anions. Two of the four $(\text{hmds})^-$ ligands act as terminal ligands to the outer Mn atoms (Mn1 and Mn1'), while the two other ligand molecules bridge the Mn1–Mn2 edges opposite to the $\eta^2\text{-}\eta^2\text{-}\eta^2\text{-}\mu^3\text{-Bi}_2^{2-}$ units. In comparison with the free Bi_2^{2-} dumbbell, the Bi–Bi distance has again been expanded to

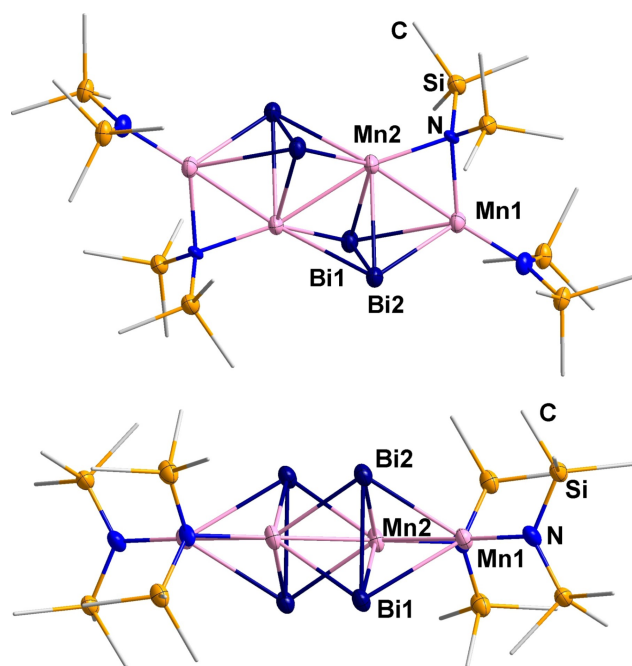


Figure 4. Molecular structure of the anion in **3** in two perpendicular views. Thermal ellipsoids of Bi, Mn, N, and Si atoms are drawn with 50% probability, with C atoms are drawn as wires. Selected distances in **3** [Å]: Bi–Bi 2.9993(10), Bi–Mn1 2.934(2) and 2.966(2), Bi–Mn2 2.842(2)–2.887(2), Mn1–Mn2 2.720(3), Mn2–Mn2' 2.804(4), Mn–(μ -N) 2.108(10) and 2.218(10), Mn–N 2.051(10).

2.9993(10) Å, in agreement with its role as a μ^3 -bridging ligand (as compared to the μ -bridging role in the anion in **2**). Hence, this result indicates the most significant involvement of this $\{\text{Bi}_2\}$ unit in coordination of the transition metal atoms. The anion in **3** can be regarded as a secondary product of the formation of **2**—whose formation might be explained by dimerization of **2** under release of four $(\text{hmds})^-$ groups. Further, a $2e^-$ reduction takes place, most probably with the aid of either additional Bi_2^{2-} or the reactant $(\text{TrBi}_3)^{2-}$ (Tr=Ga, In). Any attempts of monitoring the formation of **2** or **3** was prohibited by the paramagnetic nature of the reaction mixtures as well as immediate decomposition of the compounds under ESI-MS conditions. Side-products that were secured during these reactions are $[\text{K}(\text{crypt})][\text{Mn}(\text{hmds})_3]$ and Hhmds, and explain the fate of the $(\text{hmds})^-$ groups that left the coordination sphere of Mn^{2+} as compared to the original $[\text{Mn}(\text{hmds})_2]$ complex during the formation of **3**. The Hhmds molecules are most likely formed from deprotonation of crystal solvent (en) present in the employed Zintl salts $[\text{K}(\text{crypt-222})]_2\text{-}(\text{TrBi}_3) \cdot \text{en}$.

Formally, the transition metal atoms represent a $\{\text{Mn}_4\}^{6+}$ unit in **3**. The different coordination modes of the $(\text{hmds})^-$ groups suggest differences in the formal charges of the individual Mn atoms. The outer Mn atoms are coordinated by a terminal and a μ -bridging $(\text{hmds})^-$ ligand (and one μ^3 -bridging Bi_2^{2-} anion), while the two inner Mn atoms are coordinated by one μ -bridging $(\text{hmds})^-$ group (and two μ^3 -bridging Bi_2^{2-} units). When counting the effective charge of a terminal $(\text{hmds})^-$ anion as -1 , that of a μ -bridging $(\text{hmds})^-$ anion as $-1/2$, and that of a μ^3 -bridging Bi_2^{2-} unit as $-2/3$, it is obvious that the outer Mn atoms need to compensate for more negative charges (a total of $-2^{1/3}$) than the inner Mn atoms (a total of $-1^{1/3}$) in their direct coordination environment (disregarding the additional two negative charges of the entire cluster). This suggests that the outer atoms are closer to a formal +II oxidation state, while the inner ones can be viewed as Mn(+I). The different coordination modes should thus affect the electronic structure and bonding as well as magnetic interactions within these anions. The combination of two Mn^+ ions (Mn1 and Mn1'; $S=2$) with two Mn^{2+} ions (Mn2 and Mn2'; $S=5/2$) can afford a total spin of $S=0$ for a maximum of antiferromagnetic interactions, or a total spin of $S=9$ for ferromagnetic coupling only, or a spin state in between in a more complex case. In theory, this should be distinguishable by magnetic or ESR measurements. However, as the crystals grow on the bottom of the Schlenk tube in very low yields within metal powder, we were not able to isolate enough pure substance for these kinds of experiments so far. DFT calculations were thus undertaken to rationalize the different formal charges and to better understand the electronic situations and potential magnetic coupling schemes in the cluster anion in **3**. For the structure obtained by XRD, we calculated a high-spin state (hs) with a total of 18 unpaired electrons and a broken-symmetry (bs) state with alternating surplus of electrons of the spin types (α vs. β) at the four Mn atoms. The bs state turned out to be favored over hs by 75 kJ mol^{-1} , which is a strong indication for antiferromagnetic coupling between

the magnetic Mn sites in this case. Moreover, the HOMO–LUMO gap is much larger for bs (1.85 eV) than for hs (1.13 eV). Mulliken population analyses indicated that a clear assignment of oxidation states is difficult though. The two inner Mn atoms indeed show a slightly higher population of d orbitals (5.58 electrons each) than the two outer Mn atoms (5.41 electrons each), but a localization procedure yields either five α spin or five β spin orbitals at each of the four Mn atoms. The electrons of the corresponding minority spin are rather localized in bonds to the Bi atoms, which reminds of the situation in **2**. In turn, like in **2** but even more pronounced, the bond order of the Bi–Bi bonds is reduced (Wiberg index 0.87) and the bond length is increased by 1.23 Å as compared to Bi_2^{2-} , in excellent agreement with the experimental observation ($\Delta d = 1.78$ Å).

Finally, the work indicates the different synthetic behavior of the three binary anions under the given reaction conditions. Attempts to explore this by considering corresponding exchange reactions (see Supporting Information) indicated, however, that the reasons for this observation seem to be manifold. While the different bonding energies within the starting material and in the product molecules may control the course of the formation reactions, the formation of solid by-products on the one hand and the observation of the products in crystalline form on the other hand seem to be very important parameters that are difficult to model. We refer to future work into this direction, which requires comprehensive considerations of both molecular as well as solid-state energies and exceeds the scope of this work.

Conclusion

In the work presented herein, we report a new synthetic approach to Zintl chemistry in common organic solvents, which additionally afforded new multimetallic Zintl clusters. We combined two seemingly contradictory systems—namely salts of binary Tr/Bi Zintl anions (Tr = Ga, In, or Tl), with their known exclusive solubility in highly polar solvents, and the low-coordinate complex $[\text{Mn}(\text{hmds})_2]$, which is susceptible to such solvents but well-soluble in THF. We demonstrated that the combination of both in THF not only yields a nice reactive solution instantly, but also leads to the formation of new types of ternary or binary Zintl clusters comprising 6, 4, or 8 metal atoms of the elemental combinations Mn/Tl/Bi or Mn/Bi, respectively. We elucidated in a combined experimental and theoretical study the formation, the geometric, and the uncommon electronic structures of the new clusters $[\{(\text{hmds})_2\text{Mn}\}_2(\text{TlBi}_3)]^{2-}$ (in **1**), $[\{(\text{hmds})_2\text{Mn}\}_2(\text{Bi}_2)]^{2-}$ (in **2**), and $[\{(\text{hmds})\text{Mn}\}_4(\text{Bi}_2)_2]^{2-}$ (in **3**). This—among others—revealed **1** to be the first compound with the $(\text{TlBi}_3)^{2-}$ anion as a ligand to transition metal ions, and indicated the likeliness of weak ferromagnetic interactions of the Mn^{2+} ions via a $\mu\text{-Bi}_2^{2-}$ bridge in the diamond-shaped bimetallic unit in **2**. Moreover, the anion in **3** represents a very uncommon heteroatomic cluster based on a (formally) mixed-valent $\{\text{Mn}^{\text{I}}_2\text{Mn}^{\text{II}}_2\}$ unit bridged by two Bi_2^{2-} units, which together can be viewed as a dimeric

version of the anion in **2** upon release of two $(\text{hmds})^-$ ligands and a concomitant 2-e^- reduction. This provides an idea of how such binary polyanions grow further. As was shown by ESI mass spectrometry and magnetic measurements the compounds are comparably sensitive—which is in agreement with the observation of relatively low energy barriers calculated for structural changes.

For applying the newly formed clusters in subsequent reactions, future work will also address other types of transition metal ions and ligands involved in the low-coordinate complexes and the use of other binary p-block (semi)metal anions. Preliminary studies already indicated that this concept can be successfully expanded to many other d-block/p-block elemental combinations.

Acknowledgements

The work was supported by the German Research Foundation (Deutsche Forschungsgemeinschaft, DFG), the University of Bordeaux, the Région Nouvelle Aquitaine, Quantum Matter Bordeaux (QMBx) and the CNRS. We thank Dr. R. J. Wilson for help with the elemental analyses. Open Access funding enabled and organized by Projekt DEAL.

Conflict of Interest

The authors declare no conflict of interest.

Data Availability Statement

The data that support the findings of this study are available in the supplementary material of this article.

Keywords: Binary Zintl Anions · Bismuth · DFT Calculations · Manganese Compounds · Triel Elements

- [1] S. C. Sevov, J. M. Goicoechea, *Organometallics* **2006**, *25*, 5678.
- [2] S. Scharfe, T. F. Fässler, *Philos. Trans. R. Soc. A* **2010**, *368*, 1265.
- [3] S. Scharfe, F. Kraus, S. Stegmaier, A. Schier, T. F. Fässler, *Angew. Chem. Int. Ed.* **2011**, *50*, 3630; *Angew. Chem.* **2011**, *123*, 3712.
- [4] B. Weinert, S. Dehnen in *Clusters- Contemporary Insight in Structure and Bonding* (Ed.: S. Dehnen), Springer, Berlin, **2017**.
- [5] R. J. Wilson, N. Lichtenberger, B. Weinert, S. Dehnen, *Chem. Rev.* **2019**, *119*, 8506.
- [6] a) M. Bädler, H. Ternberger, W. Faber, J. Hahn, *Z. Naturforsch. B* **1979**, *34*, 1690; b) H. G. Von Schnering, D. Fenske, W. Höhle, M. Binnewies, K. Peters, *Angew. Chem. Int. Ed. Engl.* **1979**, *18*, 679; *Angew. Chem.* **1979**, *91*, 755; c) R. S. P. Turbervill, J. M. Goicoechea, *Chem. Rev.* **2014**, *114*, 10807.
- [7] a) M. W. Hull, S. C. Sevov, *Angew. Chem. Int. Ed.* **2007**, *46*, 6695; *Angew. Chem.* **2007**, *119*, 6815; b) M. W. Hull, A. Ugrinov, I. Petrov, S. C. Sevov, *Inorg. Chem.* **2007**, *46*, 2704; c) M. W. Hull, S. C. Sevov, *J. Am. Chem. Soc.* **2009**, *131*, 9026; d) M. W. Hull, S. C. Sevov, *Inorg. Chem.* **2007**, *46*, 10953;

- e) D. J. Chapman, S. C. Sevov, *Inorg. Chem.* **2008**, *47*, 6009; f) M. M. Gillett-Kunnath, I. Petrov, S. C. Sevov, *Inorg. Chem.* **2010**, *49*, 721; g) F. Li, S. C. Sevov, *Inorg. Chem.* **2012**, *51*, 2706; h) M. W. Hull, S. C. Sevov, *J. Organomet. Chem.* **2012**, *721–722*, 85; i) F. Li, S. C. Sevov, *Inorg. Chem.* **2015**, *54*, 8121; j) S. Frischhut, W. Klein, M. Drees, T. F. Fässler, *Chem. Eur. J.* **2018**, *24*, 9009; k) F. S. Geitner, W. Klein, T. F. Fässler, *Angew. Chem. Int. Ed.* **2018**, *57*, 14509; *Angew. Chem.* **2018**, *130*, 14717; l) F. S. Geitner, C. Wallach, T. F. Fässler, *Chem. Eur. J.* **2018**, *24*, 4103.
- [8] a) F. Li, A. Muñoz-Castro, S. C. Sevov, *Angew. Chem. Int. Ed.* **2012**, *51*, 8581; *Angew. Chem.* **2012**, *124*, 8709; b) M. W. Hull, S. C. Sevov, *Chem. Commun.* **2012**, *48*, 7720; c) F. Li, S. C. Sevov, *J. Am. Chem. Soc.* **2014**, *136*, 12056; d) F. Li, A. Muñoz-Castro, S. C. Sevov, *Angew. Chem. Int. Ed.* **2016**, *55*, 8630; *Angew. Chem.* **2016**, *128*, 8772; e) K. Mayer, L. J. Schiegerl, T. F. Fässler, *Chem. Eur. J.* **2016**, *22*, 18794; f) F. S. Geitner, J. V. Dums, T. F. Fässler, *J. Am. Chem. Soc.* **2017**, *139*, 11933.
- [9] B. Zhou, M. S. Denning, C. Jones, J. M. Goicoechea, *Dalton Trans.* **2009**, 1571.
- [10] B. Zhou, M. S. Denning, T. A. D. Chapman, J. M. Goicoechea, *Inorg. Chem.* **2009**, *48*, 2899.
- [11] F. S. Geitner, T. F. Fässler, *Chem. Commun.* **2017**, *53*, 12974.
- [12] a) B. W. Eichhorn, R. C. Haushalter, W. T. Pennington, *J. Am. Chem. Soc.* **1988**, *110*, 8704; b) B. W. Eichhorn, R. C. Haushalter, *J. Chem. Soc. Chem. Commun.* **1990**, 937; c) B. Kesanlı, J. Fettinger, B. Eichhorn, *Chem. Eur. J.* **2001**, *7*, 5277; d) J. Campbell, H. P. A. Mercier, H. Franke, D. P. Santry, D. A. Dixon, G. J. Schrobilgen, *Inorg. Chem.* **2002**, *41*, 86; e) L. Yong, S. D. Hoffmann, T. F. Fässler, *Eur. J. Inorg. Chem.* **2005**, 3663.
- [13] S. Stegmaier, M. Waibel, A. Henze, L.-A. Jantke, A. J. Karttunen, T. F. Fässler, *J. Am. Chem. Soc.* **2012**, *134*, 14450.
- [14] a) J. M. Goicoechea, S. C. Sevov, *Organometallics* **2006**, *25*, 4530; b) Z.-M. Sun, Y.-F. Zhao, J. Li, L.-S. Wang, *J. Cluster Sci.* **2009**, *20*, 601; c) J.-Q. Wang, S. Stegmaier, B. Wahl, T. F. Fässler, *Chem. Eur. J.* **2010**, *16*, 1793; d) S. Scharfe, T. F. Fässler, *Eur. J. Inorg. Chem.* **2010**, 1207; e) D. O. Downing, P. Zavaliy, B. W. Eichhorn, *Eur. J. Inorg. Chem.* **2010**, 890; f) M. Waibel, F. Kraus, S. Scharfe, B. Wahl, T. F. Fässler, *Angew. Chem. Int. Ed.* **2010**, *49*, 6611; *Angew. Chem.* **2010**, *122*, 6761; g) M. Waibel, G. Raudaschl-Sieber, T. F. Fässler, *Chem. Eur. J.* **2011**, *17*, 13391; h) T. Henneberger, W. Klein, J. V. Dums, T. F. Fässler, *Chem. Commun.* **2018**, *54*, 12381.
- [15] F. S. Geitner, W. Klein, T. F. Fässler, *Dalton Trans.* **2017**, *46*, 5796.
- [16] a) V. Queneau, S. C. Sevov, *J. Am. Chem. Soc.* **1997**, *119*, 8109; b) U. Zachwieja, J. Müller, J. Wlodarski, *Z. Anorg. Allg. Chem.* **1998**, *624*, 853; c) A. Nienhaus, R. Hauptmann, T. F. Fässler, *Angew. Chem. Int. Ed.* **2002**, *41*, 3213; *Angew. Chem.* **2002**, *114*, 3352; d) A. Spiekermann, S. D. Hoffmann, F. Kraus, T. F. Fässler, *Angew. Chem. Int. Ed.* **2007**, *46*, 1638; *Angew. Chem.* **2007**, *119*, 1663; e) M. S. Denning, J. M. Goicoechea, *Dalton Trans.* **2008**, 5882; f) B. Zhou, M. S. Denning, T. A. D. Chapman, J. E. McGrady, J. M. Goicoechea, *Chem. Commun.* **2009**, 7221; g) J.-Q. Wang, B. Wahl, T. F. Fässler, *Angew. Chem. Int. Ed.* **2010**, *49*, 6592; *Angew. Chem.* **2010**, *122*, 6742; h) C. B. Benda, M. Waibel, T. Köchner, T. F. Fässler, *Chem. Eur. J.* **2014**, *20*, 16738; i) M. M. Bentlohner, L.-A. Jantke, T. Henneberger, C. Fischer, K. Mayer, W. Klein, T. F. Fässler, *Chem. Eur. J.* **2016**, *22*, 13946; j) K. Mayer, L.-A. Jantke, S. Schulz, T. F. Fässler, *Angew. Chem. Int. Ed.* **2017**, *56*, 2350; *Angew. Chem.* **2017**, *129*, 2390; k) S. Mitzinger, J. Bandemehr, K. Reiter, J. Scott McIndoe, X. Xie, F. Weigend, J. F. Corrigan, S. Dehnen, *Chem. Commun.* **2018**, *54*, 1421.
- [17] F. X. Pan, L. J. Li, Z. M. Sun, *Chin. J. Struct. Chem.* **2016**, *35*, 1099.
- [18] F. Lips, I. Schellenberg, R. Pöttgen, S. Dehnen, *Chem. Eur. J.* **2009**, *15*, 12968.
- [19] N. Lichtenberger, N. Spang, A. Eichhöfer, S. Dehnen, *Angew. Chem. Int. Ed.* **2017**, *56*, 13253; *Angew. Chem.* **2017**, *129*, 13436.
- [20] D. Huang, J. D. Corbett, *Inorg. Chem.* **1998**, *37*, 5007.
- [21] B. Weinert, A. R. Eulenstein, R. Ababei, S. Dehnen, *Angew. Chem. Int. Ed.* **2014**, *53*, 4704; *Angew. Chem.* **2014**, *126*, 4792.
- [22] Deposition Numbers 2190219 (for **1**), 2190220 (for **2**), and 2190221 (for **3**) contain the supplementary crystallographic data for this paper. These data are provided free of charge by the joint Cambridge Crystallographic Data Centre and Fachinformationszentrum Karlsruhe Access Structures service.
- [23] L. Xu, S. Bobev, J. El-Bahraoui, S. C. Sevov, *J. Am. Chem. Soc.* **2000**, *122*, 1838.
- [24] F. Pan, S. Wei, L. Guggolz, A. R. Eulenstein, F. Tambornino, S. Dehnen, *J. Am. Chem. Soc.* **2021**, *143*, 7176.
- [25] L. Xu, S. C. Sevov, *Inorg. Chem.* **2000**, *39*, 5383.
- [26] N. V. Tkachenko, X.-W. Zhang, L. Qiao, C.-C. Shu, D. Steglenko, A. Muñoz-Castro, Z.-M. Sun, A. I. Boldyrev, *Chem. Eur. J.* **2020**, *26*, 2073.
- [27] L. Guggolz, S. Dehnen, *Chem. Eur. J.* **2020**, *26*, 11819.
- [28] B. Weinert, F. Müller, K. Harms, R. Clérac, S. Dehnen, *Angew. Chem. Int. Ed.* **2014**, *53*, 11979; *Angew. Chem.* **2014**, *126*, 12173.
- [29] B. Weinert, F. Weigend, S. Dehnen, *Chem. Eur. J.* **2012**, *18*, 13589.
- [30] N. Lichtenberger, Y. J. Franzke, W. Massa, F. Weigend, S. Dehnen, *Chem. Eur. J.* **2018**, *24*, 12022.
- [31] a) N. Lichtenberger, R. J. Wilson, A. R. Eulenstein, W. Massa, R. Clérac, F. Weigend, S. Dehnen, *J. Am. Chem. Soc.* **2016**, *138*, 9033; b) A. R. Eulenstein, Y. J. Franzke, N. Lichtenberger, R. J. Wilson, H. L. Deubner, F. Kraus, R. Clérac, F. Weigend, S. Dehnen, *Nat. Chem.* **2021**, *13*, 149; c) N. Lichtenberger, W. Massa, S. Dehnen, *Angew. Chem. Int. Ed.* **2019**, *58*, 3222; *Angew. Chem.* **2019**, *131*, 3256.
- [32] TURBOMOLE V7.6 2021, a development of University of Karlsruhe and Forschungszentrum Karlsruhe GmbH, 1989–2007, TURBOMOLE GmbH, since 2007; available from <https://www.turbomole.org>.
- [33] J. Tao, J. P. Perdew, V. N. Staroverov, G. E. Scuseria, *Phys. Rev. Lett.* **2003**, *91*, 146401.
- [34] F. Weigend, R. Ahlrichs, *Phys. Chem. Chem. Phys.* **2005**, *7*, 3297.
- [35] a) A. Klamt, G. Schüürmann, *J. Chem. Soc., Perkin Trans.* **1993**, *2*, 799; b) A. Schäfer, A. Klamt, D. Sattel, J. C. W. Lohrenz, F. Eckert, *Phys. Chem. Chem. Phys.* **2000**, *2*, 2187.
- [36] a) A. L. Allred, E. G. Rochow, *J. Inorg. Nucl. Chem.* **1958**, *5*, 264; b) E. J. Little, M. M. Jones, *J. Chem. Educ.* **1960**, *37*, 231.
- [37] a) R. Beltrán-Suito, V. Forstner, J. N. Hausmann, S. Mebs, J. Schmidt, I. Zaharieva, K. Laun, I. Zebger, H. Dau, P. W. Menezes, et al., *Chem. Sci.* **2020**, *11*, 11834; b) W. J. Evans, T. A. Ulibarri, J. W. Ziller, *J. Am. Chem. Soc.* **1988**, *110*, 6877.
- [38] W. J. Evans, S. L. Gonzales, J. W. Ziller, *J. Am. Chem. Soc.* **1991**, *113*, 9880.
- [39] C. Schoo, S. Bestgen, A. Egeberg, S. Klementyeva, C. Feldmann, S. N. Konchenko, P. W. Roesky, *Angew. Chem. Int. Ed.* **2018**, *57*, 5912; *Angew. Chem.* **2018**, *130*, 6015.
- [40] C. Schoo, S. Bestgen, A. Egeberg, J. Seibert, S. N. Konchenko, C. Feldmann, P. W. Roesky, *Angew. Chem. Int. Ed.* **2019**, *58*, 4386; *Angew. Chem.* **2019**, *131*, 4430.
- [41] B. M. Gardner, G. Balázs, M. Scheer, A. J. Wooles, F. Tuna, E. J. L. McInnes, J. McMaster, W. Lewis, A. J. Blake, S. T. Liddle, *Angew. Chem. Int. Ed.* **2015**, *54*, 15250; *Angew. Chem.* **2015**, *127*, 15465.
- [42] W. Clegg, N. A. Compton, R. Errington, N. C. Norman, *Polyhedron* **1988**, *7*, 2239.
- [43] J. R. Harper, A. L. Rheingold, *J. Organomet. Chem.* **1990**, *390*, c36.

- [44] D. Fenske, H. Fleischer, C. Persau, *Angew. Chem. Int. Ed. Engl.* **1989**, *28*, 1665; *Angew. Chem.* **1989**, *101*, 1740.
- [45] G. Hierlmeier, A. Hinz, R. Wolf, J. M. Goicoechea, *Angew. Chem. Int. Ed.* **2018**, *57*, 431; *Angew. Chem.* **2018**, *130*, 439.
- [46] P. J. Chirik, L. M. Henling, J. E. Bercaw, *Organometallics* **2001**, *20*, 534.
- [47] S. Demir, M. I. Gonzalez, L. E. Darago, W. J. Evans, J. R. Long, *Nat. Commun.* **2017**, *8*, 2144.
- [48] C. G. Werncke, E. Suturina, P. C. Bunting, L. Vendier, J. R. Long, M. Atanasov, F. Neese, S. Sabo-Etienne, S. Bontemps, *Chem. Eur. J.* **2016**, *22*, 1668.

Manuscript received: July 20, 2022

Accepted manuscript online: August 25, 2022

Version of record online: September 15, 2022

Supporting Information

Reactive Solubilization of Heterometallic Clusters by Treatment of $(\text{TrBi}_3)^{2-}$ Anions (Tr = Ga, In, Tl) with $[\text{Mn}\{\text{N}(\text{SiMe}_3)_2\}_2]$

J. Rienmüller, A. Schmidt, N. J. Yutronkie, R. Clérac, C. G. Werncke, F. Weigend*, S. Dehnen**

Table of Contents

1	Experimental Details.....	2
2	Single-Crystal Diffraction and Refinement Data.....	3
3	Micro-X-Ray Fluorescence Spectroscopy (μ -XFS)	6
4	Quantum Chemical Calculations	8
5	Attempts to Measure the Magnetic Behavior of Compound 2	12
6	References.....	13

1 Experimental Details

1.1 General Methods

All syntheses were performed under exclusion of air and moisture using standard Schlenk or glovebox techniques. Ethane-1,2-diamine (en), was distilled from CaH₂ and stored over 4 Å molecular sieves. Tetrahydrofuran (THF), diethyl ether (Et₂O), *n*-pentane and *n*-hexane, were distilled from potassium and stored over 4 Å molecular sieves. Crypt-222^[1] was dried *in vacuo* for 12 hours. Ternary solids K₅Tr₂Bi₄ (Tr = Ga, In, Bi) were synthesized and extracted in en as described previously.^[2] [Mn(hmds)₂] was synthesized by addition of Khmds to MnCl₂ in THF according to a literature protocol.^[3]

1.2 Preparation of [K(crypt222)]₂[(hmds)₂Mn]₂(TlBi₃)·1.5Et₂O (1): [K(crypt-222)]₂(TlBi₃) (30.00 mg, 18.05 μmol) were added to [Mn(hmds)₂] (26 mg, 36.09 μmol) in a brown glass vial in a glovebox and dissolved in 2 mL of a 1:1 mixture (v:v) of Et₂O and THF. After stirring for 5 min, the suspension was filtered. The dark brown solution was layered with 2 ml of *n*-hexane and stored at -40°C. After one week, small dark-brown plank-shaped crystals of **1** crystallized (yield: ~10%) at the bottom of the Schlenk tube besides a large amount of colorless crystals of [K(crypt-222)][Mn(hmds)₃].

1.3 Preparation of [K(crypt-222)]₂[(hmds)₂Mn]₂(Bi₂)·4THF (2): [K(crypt-222)]₂(GaBi₃) (38 mg, 24.87 μmol) or [K(crypt-222)]₂(InBi₃) (38 mg, 23.27 μmol) were added to [Mn(hmds)₂] (35 mg, 48.33 μmol) in a brown glass vial in a glovebox and dissolved in 1.5 mL of THF. After stirring for 5 min, the suspension was filtered. The dark brown solution was layered with 2 ml of *n*-hexane and stored at -40°C. After one week, large dark-brown plank-shaped crystals of **2** (yield: ~30%), which were covered with a powdery precipitate, crystallized at the bottom of the Schlenk tube.

1.4 Preparation of [K(crypt-222)]₂[(hmds)₂Mn]₄(Bi₂)₂ (3): [K(crypt-222)]₂(GaBi₃) (38 mg, 24.87 μmol) or [K(crypt-222)]₂(InBi₃) (38 mg, 23.27 μmol) were added to [Mn(hmds)₂] (40.00 mg, 55.23 μmol) in a brown glass vial in a glovebox and dissolved in 1.5 mL of THF. After 30 min, the suspension was filtered. The dark brown solution was layered with 2 ml of *n*-hexane and stored at -40°C. After a few days, small dark-red irregularly shaped crystals of **3** (yield: ~15%), which were covered with a powdery precipitate, appeared at the bottom of the Schlenk tube.

2 Single-Crystal Diffraction and Refinement Data

2.1 Crystal Measurement and Refinement Details

The data sets were collected on a Bruker D8 Quest with microfocus source emitting $\text{MoK}\alpha$ radiation ($\lambda = 0.71073 \text{ \AA}$) and a Photon 100 detector at $T = 100 \text{ K}$. The structures were solved by dual space methods of SHELXT-2018/2 within the Olex2-1.3 software^[4–6] and refined using least-squares procedures on a F^2 with SHELXL-2018/3 in Olex2.^[6,7,4] General crystallographic data are listed in Table S1.

Table S1: Crystal data and details of the structure determination of 1 – 3.

Compound	1·1.5Et ₂ O	2·4THF	3
empirical formula	C _{64.50} H _{146.50} Bi ₃ K ₂ Mn ₂ N ₈ O _{12.50} Si ₈ Tl	C ₆₈ H ₁₆₀ Bi ₂ K ₂ Mn ₂ N ₈ O ₁₄ Si ₈	C ₆₀ H ₁₄₄ Bi ₄ K ₂ Mn ₄ N ₈ O ₁₂ Si ₈
chemical formula	[K(crypt222)] ₂ ·[{(hmds) ₂ Mn} ₂ ·(TlBi ₃)]·1.5Et ₂ O	[K(crypt-222)] ₂ ·[{(hmds) ₂ Mn} ₂ (Bi ₂)]·4THF	[K(crypt-222)] ₂ ·[{(hmds)Mn} ₄ (Bi ₂) ₂]
emp. formula weight [g mol ⁻¹]	2488.05	2144.79	2528.42
temperature [K]	100	100	100
crystal color, shape	dark-red irregular block	dark brown plank	dark black irregular block
crystal system	Triclinic	monoclinic	triclinic
space group	$P\bar{1}$ (Nr. 2)	$C2/c$ (Nr.15)	$P\bar{1}$ (Nr. 2)
<i>a</i> [Å]	14.532(2)	26.3859(10)	11.8800(17)
<i>b</i> [Å]	15.288(3)	16.6339(5)	14.941(3)
<i>c</i> [Å]	26.852(4)	26.1946(10)	16.334(5)
α [°]	82.277(6)	90	66.01(3)
β [°]	74.809(4)	112.4840(10)	73.461(14)
γ [°]	62.273(5)	90	66.837(9)
<i>V</i> [Å ³]	5095.5(14)	10622.9(7)	2408.5(10)
<i>Z</i>	2	4	1
ρ_{calc} [g cm ⁻³]	1.622	1.341	1.743
μ [mm ⁻¹]	7.204	3.755	8.021
<i>F</i> (000)	2456	4408	1238
crystal size [mm ³]	0.412 × 0.278 × 0.1	0.088 × 0.141 × 0.385	0.122 × 0.133 × 0.25
radiation	MoK α ($\lambda = 0.71073 \text{ \AA}$)	MoK α ($\lambda = 0.71073 \text{ \AA}$)	MoK α ($\lambda = 0.71073 \text{ \AA}$)
2 θ range [°]	4.32 – 55.98	4.90 – 52.16	3.91 – 51.00
Index ranges	–18 ≤ <i>h</i> ≤ 19, –20 ≤ <i>k</i> ≤ 20, –35 ≤ <i>l</i> ≤ 35	–32 ≤ <i>h</i> ≤ 32, –20 ≤ <i>k</i> ≤ 20, –32 ≤ <i>l</i> ≤ 32	–14 ≤ <i>h</i> ≤ 14, –18 ≤ <i>k</i> ≤ 18, –19 ≤ <i>l</i> ≤ 19
absorption correction type	multi-scan	multi-scan	multi-scan
reflections collected	156719	90054	33278
ind. reflections / <i>R</i> _{int} / <i>R</i> _{sigma}	24433 / 0.0583 / 0.0425	10509 / 0.0446 / 0.0229	8633 / 0.0646 / 0.0642
restraints / parameters	269 / 1069	6 / 492	48 / 454
Final <i>R</i> indexes [<i>I</i> ≥ 2σ (<i>I</i>)]	<i>R</i> ₁ = 0.0332, <i>wR</i> ₂ = 0.0707	<i>R</i> ₁ = 0.0200, <i>wR</i> ₂ = 0.0407	<i>R</i> ₁ = 0.0611, <i>wR</i> ₂ = 0.153
Final <i>R</i> indexes [all data]	<i>R</i> ₁ = 0.0550, <i>wR</i> ₂ = 0.0794	<i>R</i> ₁ = 0.0271, <i>wR</i> ₂ = 0.0425	<i>R</i> ₁ = 0.1113, <i>wR</i> ₂ = 0.179
goodness-of-fit on <i>F</i> ²	1.013	1.042	1.148
max peak / hole [e Å ⁻³]	1.556 / –1.734	0.452 / –0.541	4.609 / –2.377
CCDC number	2190219	2190220	2190221

All non-hydrogen atoms were refined using anisotropic displacement parameters. All hydrogen atoms were refined by using a riding model. Absorption correcting was carried out using MULTISCAN. Supplementary structural figures are shown in Figures S1-S4. The structures were drawn with DIAMOND.^[8] They are shown with displacement ellipsoids at the 50% probability level for non-hydrogen atoms. Hydrogen atoms are not shown for clarity.

2.2 Supplementary Structural Figures

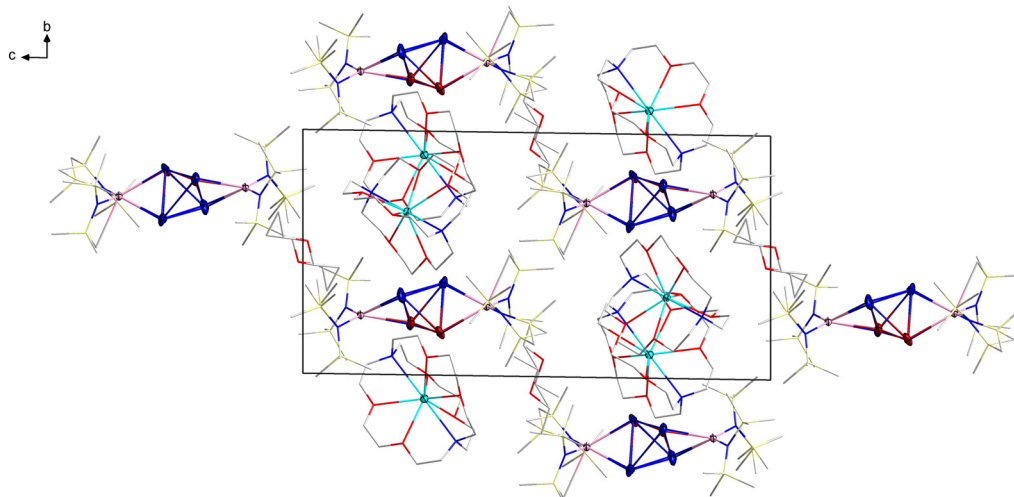


Figure S1: Unit cell of compound $1 \cdot 1.5\text{Et}_2\text{O}$. Displacement ellipsoids are shown with 50% probability for non-hydrogen atoms; hydrogen atoms are not shown for clarity.

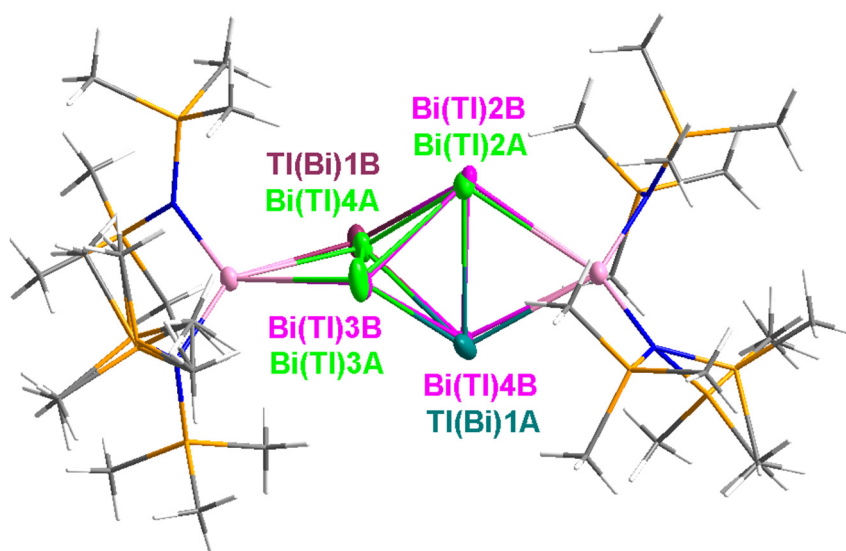


Figure S2: Molecular structure of the anion in compound $1 \cdot 1.5\text{Et}_2\text{O}$, outlining the disorder of the $\{\text{TlBi}_3\}$ unit into a set of A split positions (green/teal) and a set of B split position (pink/plum). Displacement ellipsoids of metal atoms are shown with 50% probability.

Refinement of $1 \cdot 1.5\text{Et}_2\text{O}$ led to best results, when considering a statistical disorder of the *pseudo*-tetrahedral unit over two very slightly differing sets of atomic sites (A and B) with corresponding split positions. As Tl and Bi atoms cannot be distinguished by standard X-ray

diffraction experiments, all involved atomic sites were assigned a 0.125 occupancy by Tl atoms and a 0.375 occupancy by Bi atoms. For both sets, A and B, one of the atoms was randomly picked to represent the Tl atom in Figure S2. The disorder cannot be reasonably modeled by considering a larger unit cell or a lower symmetry space group; structure solution and refinement in *P1* led to the same finding.

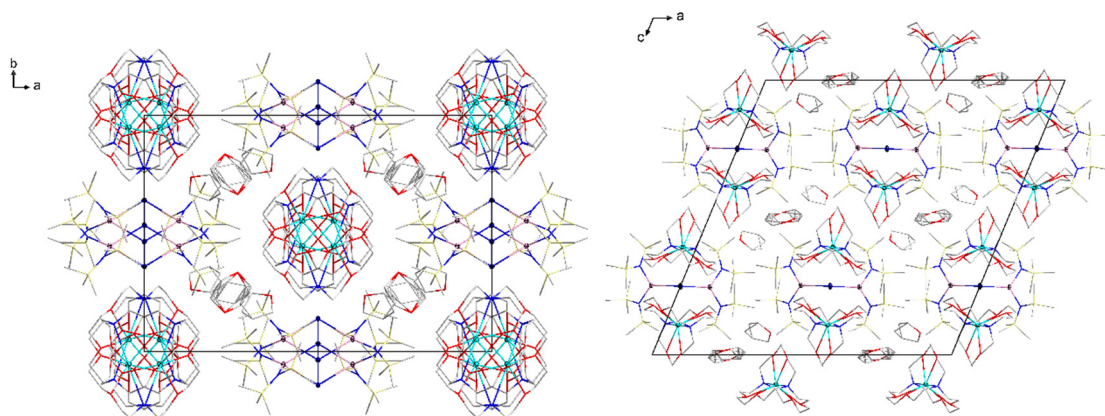


Figure S3: Fragment of the crystal structure of compound 2·4THF viewed along the crystallographic *c* and *b* axes (left-hand side and right-hand side, respectively). Displacement ellipsoids are shown with 50% probability for non-hydrogen atoms; hydrogen atoms are not shown for clarity.

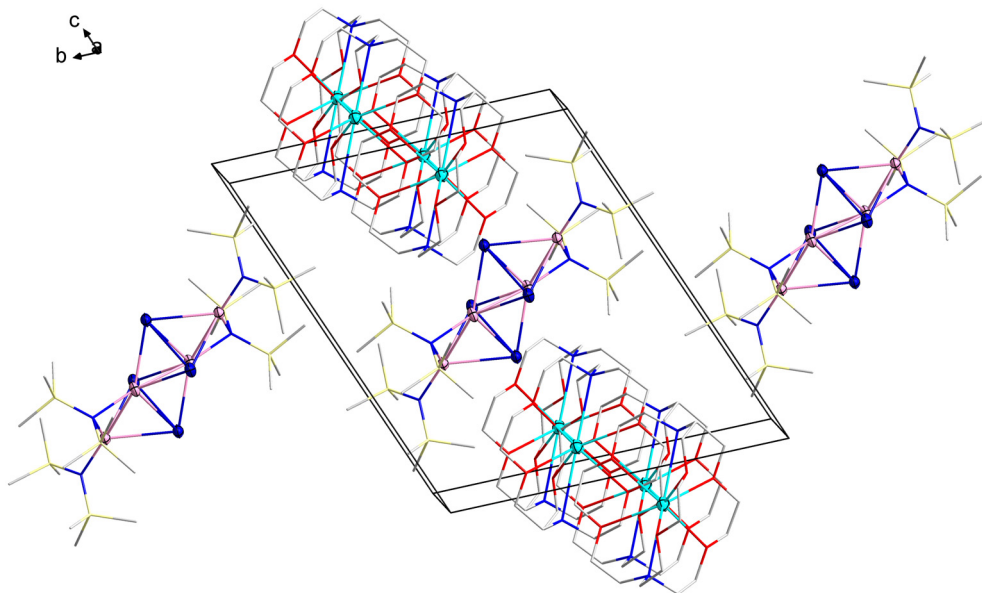


Figure S4: Fragment of the crystal structure of compound 3. Displacement ellipsoids are shown with 50% probability for non-hydrogen atoms; hydrogen atoms are not shown for clarity.

3 Micro-X-Ray Fluorescence Spectroscopy (μ -XFS)

All μ -XFS measurements were performed on a Bruker M4 Tornado, equipped with an Rh-target X-ray tube and a silicon drift detector. Quantification of the elements is achieved through deconvolution of the spectra. The results are summarized in Table S2. The rhodium content from the target is omitted from the quantification results. Figures S5-S7 show the spectra for single crystals of compounds **1**·1.5Et₂O, **2**·4THF, and **3**, respectively, along with the results of the deconvolution algorithm. Silicon and potassium contents are notoriously difficult to detect in correct amounts by means of μ -XFS, for which the values are not given here.

Table S2: Summary of the Micro X-Ray Fluorescence Spectroscopy Results

Compound	Element	Series	Element wt%	Atom %	Element ratio	
					Exp.	Calc.
1 ·1.5Et ₂ O	Mn	K	10.67	22.58	2	2.03
	Tl	L	19.53	11.11	1	1
	Bi	L	58.86	32.73	3	2.94
2 ·4THF	Mn	K	19,15	28,68	1	1.16
	Bi	L	60,68	23.88	1	1
3	Mn	K	16.84	30.07	1	1
	Bi	L	68.00	31.91	1	1.06

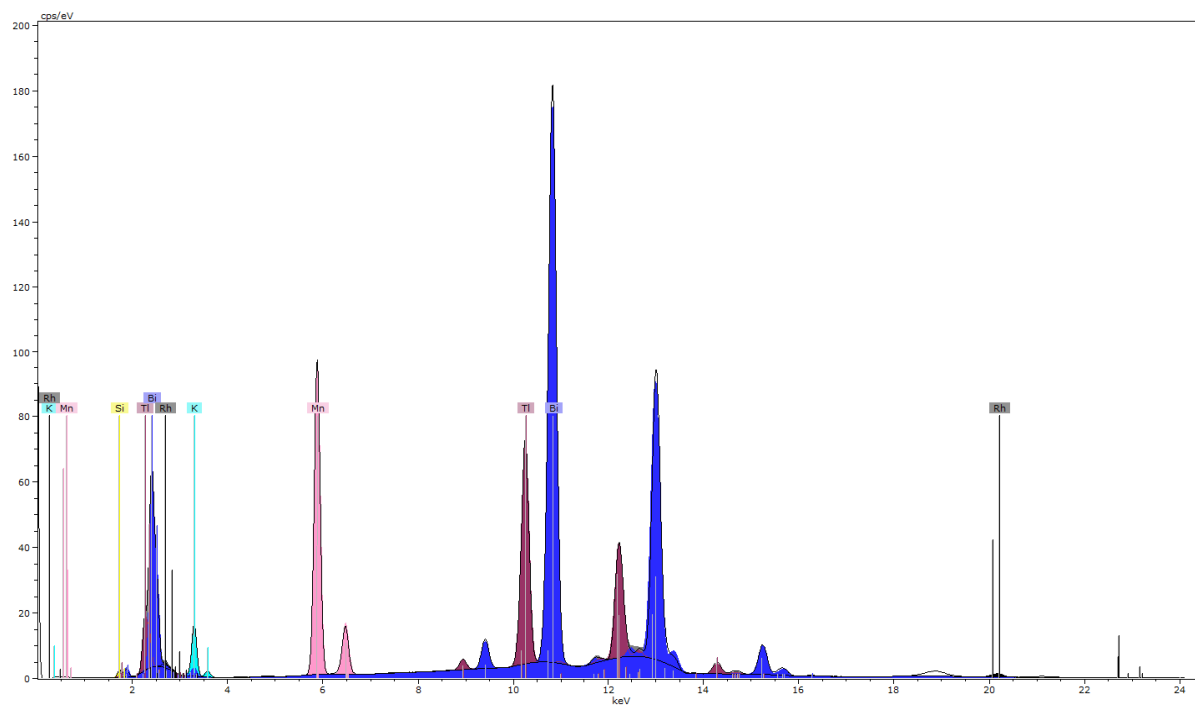


Figure S5: Micro X-ray fluorescence spectrum of compound **1·1.5Et₂O with the results of the deconvolution algorithm. The color code refers to the one used in the crystal structure figures: K (sky blue), Bi (blue), Mn (rose), Tl (red-brown), Si (yellow).**

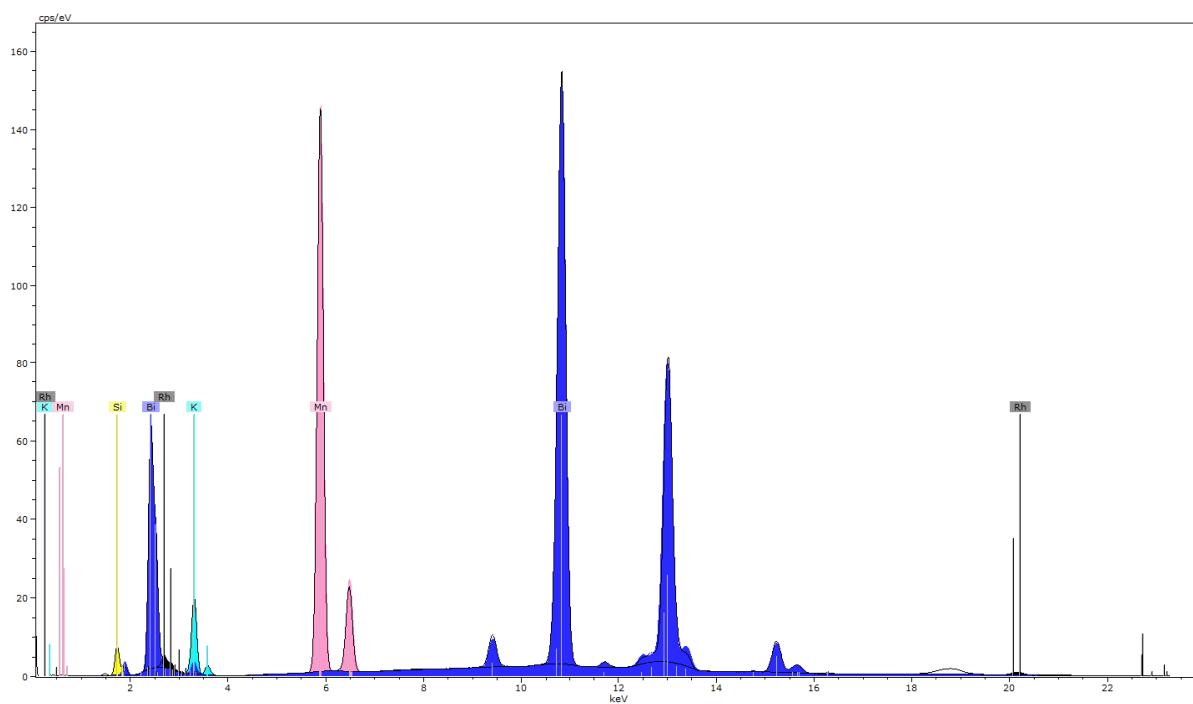


Figure S6: Micro X-ray fluorescence spectrum of compound 2·4THF with the results of the deconvolution algorithm. The color code refers to the one used in the crystal structure figures: K (sky blue), Bi (blue), Mn (rose), Si (yellow).

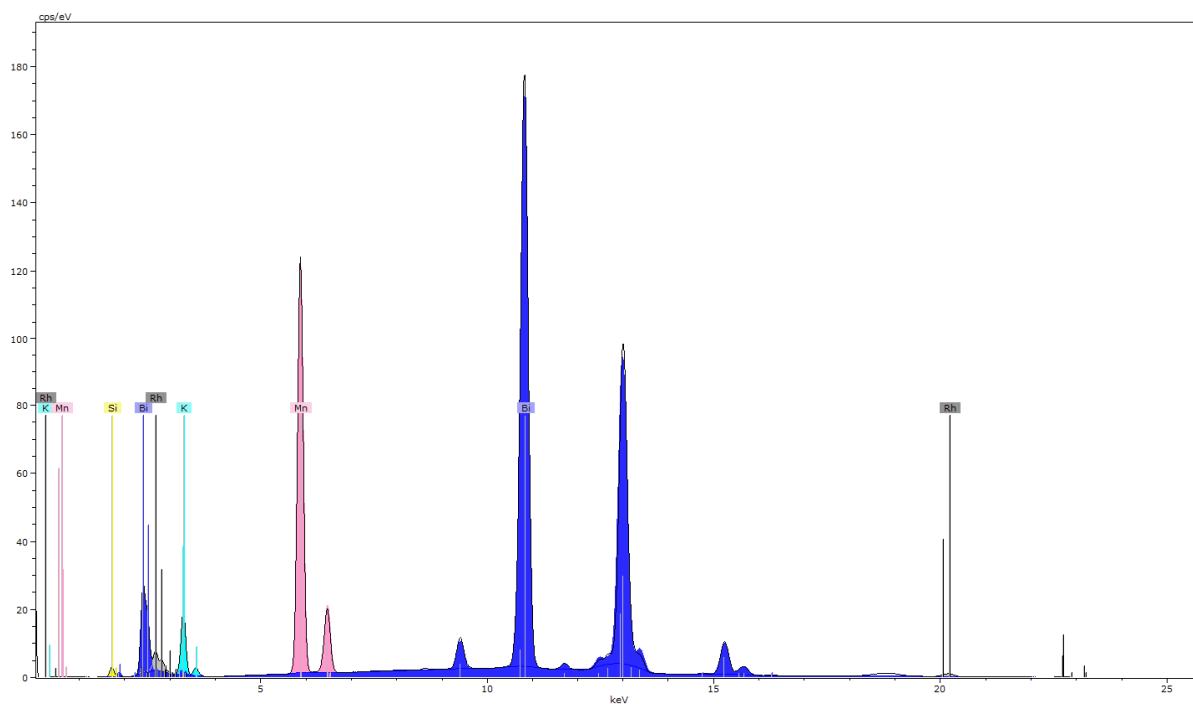


Figure S7: Micro X-ray fluorescence spectrum of compound 3 with the results of the deconvolution algorithm. The color code refers to the one used in the crystal structure figures: K (sky blue), Bi (blue), Mn (rose), Si (yellow).

4 Quantum Chemical Calculations

4.1 Methods

Density functional calculations have been performed using the program Turbomole (Version 7.5.) with the functional TPSSh.^[9] The basis set def2-TZVP^[10] has been used with the corresponding auxiliary bases and effective core potentials (ECP-60) for thallium and bismuth as well as an ECP-28 for indium.^[11] Counter ions have been modeled with the conductor-like screening model (COSMO)^[12] using standard settings and an infinite dielectric constant. Force constants and vibrational spectra were calculated using the aoforce program. The absence of any imaginary frequencies proves the structure to be a local minimum. Population analyses were performed using the method of Mulliken,^[14] bond orders were calculated using the method of Mayer and Wiberg,^[15] and molecular orbitals were plotted with Chemcraft (Version 1.8).^[16]

4.2. Structural Data, Mulliken Charges, and Numbers of Unpaired Electrons (Mn)

Table S3: Comparison of experimental and calculated interatomic distances (in Å) of the cluster anion in 1. Atom numbers refer to the ones used in Figure 2 in the main document.

Bond	Experimental	Calculated
Bi–Bi		2.974 – 3.032
Bi–Tl		3.114 – 3.283
Bi/Tl–Bi/Tl	2.805(3) – 3.314(3)	
Mn–Bi		3.019 – 3.090
Mn–Tl		3.218
Mn–Bi/Tl	2.966(3) – 3.105(3)	
Mn–N	2.037(4) – 2.051(3)	2.034 – 2.063

Table S4: Comparison of experimental and calculated interatomic distances (in Å) of the cluster anion in 2. Atom numbers refer to the ones used in Figure 2 in the main document.

Bond	Experimental	Calculated
Bi1–Bi2	2.9022(2)	2.874
Bi1–Mn1	2.9617(3)	2.928
Bi2–Mn1	2.9712(3)	2.928
Mn1–N2	2.0659(19)	2.056
Mn1–N1	2.0692(18)	2.056

Table S5: Comparison of experimental and calculated interatomic distances (in Å) of the cluster anion in 3. Atom numbers refer to the ones used in Figure 4 in the main document.

Bond	Experimental	Calculated
Bi1–Bi2	2.9993(10)	2.969
Bi1–Mn2	2.887(2)	2.864
Bi1–Mn2'	2.842(2)	2.832
Bi1–Mn1	2.966(2)	2.973
Bi2–Mn2	2.877(2)	2.856
Bi2–Mn2'	2.8468(19)	2.846
Bi2–Mn1	2.934(2)	2.953
Mn2–Mn2'	2.804(4)	2.807
Mn1–Mn2	2.720(3)	2.724

Table S6: Mulliken charges at the bismuth atoms before and after the coordination of $(\text{TrBi}_3)^{2-}$ ($\text{Tr} = \text{Ga}, \text{In}, \text{Tl}$) to $\text{Mn}(\text{hmds})_2$ and number of unpaired electrons (nue) at manganese in $\text{L}_2(\text{TrBi}_3)^{2-}$ (high-spin configuration; $\text{L} = \{(\text{hmds})_2\text{Mn}\}$).

	Mulliken charge (Bi)			nue (Mn)	
$(\text{TlBi}_3)^{2-}$	-0.57			-	
$[\text{L}_2(\text{TlBi}_3)]^{2-}$	-0.36	-0.38	-0.39	4.87	4.92
$(\text{InBi}_3)^{2-}$	-0.53			-	
$[\text{L}_2(\text{InBi}_3)]^{2-}$	-0.33	-0.33	-0.33	4.87	4.92
$(\text{GaBi}_3)^{2-}$	-0.48			-	
$[\text{L}_2(\text{GaBi}_3)]^{2-}$	-0.27	-0.28	-0.30	4.88	4.89

Table S7: Mulliken charges at the bismuth atoms before and after the coordination of $(\text{Bi}_2)^{2-}$ anions to $\text{Mn}(\text{hmds})_2$ and number of unpaired electrons (nue) at manganese in $[\text{L}_2(\text{Bi}_2)]^{2-}$ (high-spin configuration; $\text{L} = \{(\text{hmds})_2\text{Mn}\}$).

	Mulliken charge (Bi)		nue (Mn)	
$(\text{Bi}_2)^{2-}$	-1		-	
$[\text{L}_2(\text{Bi}_2)]^{2-}$	-0.58	-0.58	4.69	4.69

Table S8: Mulliken charges at the bismuth atoms before and after the coordination of two $(\text{Bi}_2)^{2-}$ anions to one $\{\text{Mn}(\text{hmds})_2\}$ and one $\{\text{Mn}(\text{hmds})_2\}^+$ moiety and number of unpaired electrons (nue) at the manganese atoms in $[\text{L}_2\text{L}'_2(\text{Bi}_2)_2]^{2-}$ ($\text{L} = \{(\text{hmds})_2\text{Mn}\}$; $\text{L}' = \{(\text{hmds})_2\text{Mn}\}^+$). Positive values indicate alpha spins, negative values indicate beta spins.

	Mulliken charge (Bi)		nue (Mn)			
$(\text{Bi}_2)^{2-}$	-1		-			
$[\text{L}_2(\text{Bi}_2)]^{2-}$	-0.42	-0.40	4.79	-4.38	4.38	-4.79

4.2 Calculated Structure of a Hypothetical Zn Analogue of Compound 2

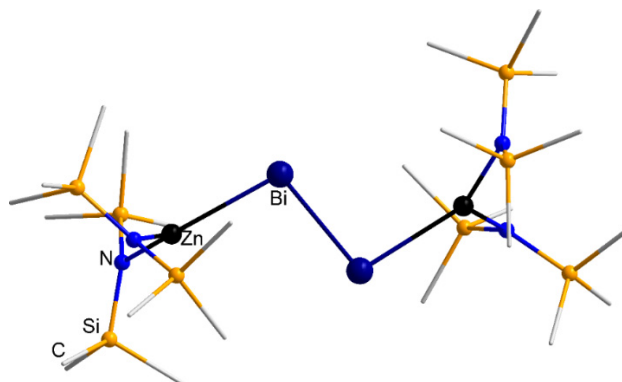
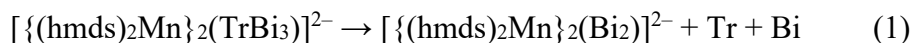


Figure S8: Calculated end-on coordination of Bi_2^{2-} upon interaction with $[\text{Zn}(\text{hmnds})_2]$ units.

4.1 Considerations on the Different Reaction Behavior of $(\text{GaBi}_3)^{2-}$, $(\text{InBi}_3)^{2-}$, and $(\text{TlBi}_3)^{2-}$

We used quantum chemical calculations to explore possible reasons why the three binary anions behave so differently in the syntheses explored in this work.

As an attempt to explore why **1** is observed for $\text{Tr} = \text{Tl}$, while starting materials with $\text{Tr} = \text{In}$ or Ga afford the anion in **2**, we calculated the energies for a reaction affording the anion in **2** from that in **1** (and their hypothetical homologues), as shown in equation (1):



Corresponding reaction energies are 461, 483, or 525 kJ/mol for $\text{Tr} = \text{Tl}$, In , or Ga , respectively. The reactions thus show a strong preference for the left-hand side (hence, the anion in **1**, and its homologues) in particular for Ga , which disagrees with the experimental observation. Matters change however, when accounting for the experimental observation of metallic deposit by including the cohesive energy of 182, 243, or 277 kJ/mol ($\text{Tr} = \text{Tl}$, In , or Ga), and 207 kJ/mol (Bi) at the right-hand side. The left-hand side now is only slightly preferred by 72, 33, or 41 kJ/mol ($\text{Tr} = \text{Tl}$, In , or Ga), with the In and Ga cases being less endoenergetic, and thus the fragmentation is more likely to occur. Additionally, one needs to take into consideration the driving force of crystallization as $[\text{K}(\text{crypt-222})]^+$ salts; it is very likely that the (negative) lattice energies associated with the crystal formation easily overcompensate the small (positive) numbers for the calculated reaction energies. In summary these studies mainly demonstrate the subtle differences between the compounds of the three triel elements, and also indicate the necessity to account for solid precipitates or crystallization in order to explain the experimental findings.

The formation of the anion in **2** was also studied in comparison with the other elemental combinations according to equation (2):



Under consideration of the cohesive energies of Tr, as done for equation (1), reaction energies are +2.5, -34.7, or -35.5 kJ/mol (Tr = Ga, In, Tl). Thus, the preference of this structure for Ga and In relative to Tl is obvious and in agreement with the experimental observations – even without consideration of lattice energies in this case, which are likely to enhance the trend for the reasons given above (and the assumption of a relatively stable salt of the highly symmetric $(\text{TrBi}_3)^{2-}$ anion).

5 Attempts to Measure the Magnetic Behavior of Compound 2

The magnetization measurements were performed on a Quantum Design MPMS-XL SQUID magnetometer operating between 1.8 and 400 K and applied dc fields of up to 7 T. The measurements were performed on microcrystalline samples (2.1, 12.9, 10.6, 9.9 and 16.2 mg) sealed in double polypropylene/polyethylene bags (with a typical size of $3 \times 0.5 \times 0.02 \text{ cm}^3$, and mass of 32.5, 18.4, 24.9, 34.3, 27.4 mg respectively) under argon. The data were corrected for the intrinsic diamagnetic contributions of the sample and the sample holder.

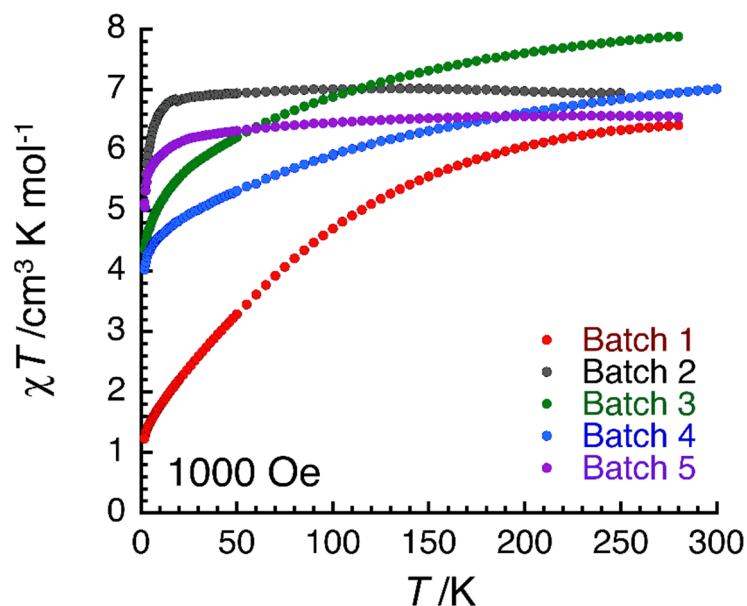


Figure S9: Temperature dependence of the χT product for the five different batches of the product obtained at the formation of compound 2 (see discussion in the main text) at 0.1 T (χ is defined as M/H per mole of complex).

6 References

- [1] 4,7,13,16,21,24-Hexaoxa-1,10-diazabicyclo[8.8.8]hexacosane.
- [2] a) L. Xu, S. C. Sevov, *Inorg. Chem.* **2000**, *39*, 5383; b) N. Lichtenberger, Y. J. Franzke, W. Massa, F. Weigend, S. Dehnen, *Chem. Eur. J.* **2018**, *24*, 12022; c) N. Lichtenberger, N. Spang, A. Eichhöfer, S. Dehnen, *Angew. Chem.* **2017**, *129*, 13436.
- [3] H. Bürger, U. Wannagat, *Monatshfte für Chemie* **1964**, *95*, 1099.
- [4] O. V. Dolomanov, L. J. Bourhis, R. J. Gildea, J. A. K. Howard, H. Puschmann, *J. Appl. Crystallogr.* **2009**, *42*, 339.
- [5] G. M. Sheldrick, *Acta Crystallogr., Sect. A: Found. Adv.* **2015**, *71*, 3.
- [6] G. M. Sheldrick, *Acta Crystallogr., Sect. A: Found. Adv.* **2008**, *64*, 112.
- [7] a) G. M. Sheldrick, *Acta Crystallogr., Sect. C: Struct. Chem.* **2015**, *71*, 3; b) G. M. Sheldrick, *ShelXL-2018*, Universität Göttingen, Göttingen (Germany), **2018**.
- [8] K. Brandenburg, *Diamond*, Crystal Impact GbR, Bonn, Germany, **2021**.
- [9] V. N. Staroverov, G. E. Scuseria, J. Tao, J. P. Perdew, *J. Chem. Phys.* **2003**, *119*, 12129.
- [10] F. Weigend, *Phys. Chem. Chem. Phys.* **2006**, *8*, 1057.
- [11] B. Metz, H. Stoll, M. Dolg, *J. Chem. Phys.* **2000**, *113*, 2563.
- [12] a) A. Klamt, G. Schüürmann, *J. Chem. Soc., Perkin Trans. 2* **1993**, 799. b) A. Schäfer, A. Klamt, D. Sattel, J. C. W. Lohrenz, F. Eckert, *Phys. Chem. Chem. Phys.* **2000**, *2*, 2187.
- [13] R. S. Mulliken, *J. Chem. Phys.* **1955**, *23*, 2338.
- [14] I. Mayer, *Chem. Phys. Lett.* **1983**, *97*, 270.
- [15] Chemcraft - graphical software for visualization of quantum chemistry computations. <https://www.chemcraftprog.com>.